

Raman optical activity and stimulated Raman scattering along the c axis in α -quartz

M. Klein, Max Maier, and W. Prettl

Naturwissenschaftliche Fakultät II—Physik, Universität Regensburg, D-8400 Regensburg, Federal Republic of Germany

(Received 24 May 1983)

Stimulated Raman scattering of the 132- and 468-cm⁻¹ optical lattice vibrations was investigated along the c axis (z direction) of α -quartz. We measured the dependence of the Raman threshold intensity on the polarization of the neodymium-doped yttrium aluminum garnet (Nd:YAG) laser pump light and on temperature from 10 to 70 K. The polarization of the stimulated Raman Stokes light was determined for different pump light polarizations. Raman optical activity was observed for the 132-cm⁻¹ mode of α -quartz. In a right-handed, optically active quartz crystal the Raman threshold intensity for left-handed, circularly polarized pump light was lower by a factor of about 1.5 than for right-handed circularly polarized light. Raman optical activity was not observed for the 468-cm⁻¹ mode within our experimental accuracy. A theory of stimulated Raman scattering including the effects of Raman optical activity is applied to quartz. Relations between the Raman circular intensity difference and the magnetic dipole and electric quadrupole polarizabilities are derived. The experimental results for both Raman modes are compared with a traveling wave and an oscillator theory of stimulated Raman scattering.

I. INTRODUCTION

Stimulated Raman scattering (SRS) in α -quartz has been studied with powerful ruby lasers at room temperature and liquid-helium temperature.¹⁻⁶ The following results were obtained. The threshold intensity of SRS is smaller at liquid-helium temperature than at room temperature.³ There is a competition between SRS from the 132-cm⁻¹ E mode and the 468-cm⁻¹ A_1 mode⁷ which depends on the propagation direction and the polarization of the pump light in the quartz crystal.^{1,3} Mode-pulling effects observed for the 468-cm⁻¹ mode indicate that the surfaces of the quartz crystal form a Raman resonator.² In addition to stimulated Raman scattering, stimulated Brillouin scattering^{1,2} was investigated, and optical damage^{1,3} of the surfaces of the crystal by the high laser intensity was found. No systematic investigation of the dependence of SRS on pump-light polarization and temperature has been carried out. The coherent excitation of polaritons in α -quartz by a two-beam method, the generation of infrared radiation, and the decay of the 468-cm⁻¹ phonons were studied in Refs. 8-11.

Recently, the threshold intensity of SRS from the 132-cm⁻¹ mode along the c axis of α -quartz was measured as a function of pump-laser polarization at liquid-helium temperature.¹² The threshold intensities of right- and left-circularly-polarized¹³ pump light differed by about a factor of 1.5. The results were explained in terms of Raman optical activity.

Raman optical activity was discovered about a decade ago in optically active substances.¹⁴⁻¹⁷ A difference in the spontaneous Raman intensities was observed for right- and left-circularly-polarized incident light. The Raman circular intensity difference is defined by¹⁶ $\Delta_{\text{spont}} = (S_r - S_l)/(S_r + S_l)$, where S_r and S_l are the spontaneous Raman intensities for right- and left-circularly-polarized

incident light, respectively. Δ_{spont} was found to be of the order of 10^{-3} for chiral molecules.^{14,15} It was shown that the interference between the molecular polarizability and optical activity tensors is responsible for Raman optical activity.¹⁷ Investigations of the Raman optical activity of chiral molecules provide structural and stereochemical information.^{14,15} Raman optical activity is complementary to optical rotatory dispersion and circular dichroism in the infrared spectral region.¹⁸

In this paper we present the results of a systematic theoretical and experimental investigation of stimulated Raman scattering and Raman optical activity for light propagation along the c axis (z direction) of α -quartz. In Sec. II the theory of stimulated Raman scattering and Raman optical activity of Oudar *et al.*¹⁹ is resumed and applied to the 132- and 468-cm⁻¹ modes of α -quartz. Expressions for the Raman circular intensity difference are derived. The threshold intensity of SRS and the polarization properties of the Raman Stokes light are treated with the use of a traveling-wave theory and an oscillator theory of SRS. In Sec. III the experimental setup is described and the experimental results are presented and discussed. The dependence of the threshold intensity of SRS on pump-laser polarization and temperature and the characteristics of the Raman Stokes polarization are investigated experimentally for the 132- and 468-cm⁻¹ modes and compared with theory. The results are summarized in Sec. IV.

II. THEORY

We describe first a traveling-wave theory for the Raman generator, in which the Stokes light is amplified during one passage through the crystal. The theory is then extended to the Raman oscillator where the end surfaces of the crystal form the resonator. The experimental re-

sults will be shown [see Sec. III B 1 (a)] to lie between the limiting cases of the Raman generator and oscillator because the end surfaces of the crystal are not perfectly parallel to one another. This fact limits the number of passages through the crystal and causes a dependence of the Raman amplification on the angle between the entrance and exit surface of the crystal.

A. General equations

1. Wave equation

The interaction of the light fields with the scattering medium is described by the wave equation¹⁹

$$\vec{\nabla} \times (\vec{\nabla} \times \vec{E}) + \frac{\vec{\epsilon}}{c_0^2} \frac{\partial^2 \vec{E}}{\partial t^2} = -\frac{4\pi}{c_0^2} \frac{\partial^2 \vec{P}^A}{\partial t^2} - \frac{4\pi}{c_0} \vec{\nabla} \times \frac{\partial \vec{M}^A}{\partial t} + \frac{2\pi}{3c_0^2} \frac{\partial^2}{\partial t^2} (\vec{\nabla} \cdot \vec{Q}^A). \quad (1)$$

\vec{E} is the electric field vector, $\vec{\epsilon}$ the dielectric tensor, and c_0 the velocity of light in vacuum. The polarization vector \vec{P}^A , the magnetization vector \vec{M}^A , and the tensor \vec{Q}^A of the electric quadrupole moment density are written as

$$\vec{P}^A = \frac{1}{4\pi} (\vec{\zeta}^{A1} \cdot \vec{\nabla}) \times \vec{E} + \vec{P}^{\text{NL}}, \quad (2a)$$

$$\vec{M}^A = \frac{1}{4\pi} \vec{\zeta}^{A2} \cdot (\vec{\nabla} \times \vec{H}) + \vec{M}^{\text{NL}} = \frac{1}{4\pi c_0} \vec{\zeta}^{A2} \cdot \frac{\partial \vec{D}}{\partial t} + \vec{M}^{\text{NL}}, \quad (2b)$$

$$\vec{Q}^A = \vec{\Lambda} \cdot \vec{E} + \vec{Q}^{\text{NL}}. \quad (2c)$$

The first terms on the right-hand sides of Eqs. (2) cause optical activity. They are discussed in detail in the next section. The second terms describe stimulated Raman scattering, including the effects of Raman optical activity.

The nonlinear polarization \vec{P}^{NL} is given to first order in u/λ , where u is a typical atomic distance and λ is the wavelength of light, by¹⁹

$$\vec{P}^{\text{NL}} = \vec{\chi}^{(3)} \cdot \vec{E} \vec{E} \vec{E} + \vec{\chi}^{\text{MD}} \cdot \vec{B} \vec{E} \vec{E} + \vec{\chi}^{\text{EQ}} \cdot \vec{\nabla} \vec{E} \vec{E} \vec{E}, \quad (3)$$

where $\vec{\chi}^{(3)}$, $\vec{\chi}^{\text{MD}}$, and $\vec{\chi}^{\text{EQ}}$ are higher-order nonlinear susceptibilities. The nonlinear magnetization \vec{M}^{NL} and the electric quadrupole moment density \vec{Q}^{NL} are assumed to be proportional to the third power of the electric field vector \vec{E} . The first term on the right-hand side of Eq. (3) leads to stimulated Raman scattering. The second and third terms of Eq. (3) together with \vec{M}^{NL} and \vec{Q}^{NL} are responsible for the effects of Raman optical activity on SRS.

To simplify the wave equation (1) we make the ansatz of plane waves with slowly varying amplitudes.²⁰ We have

$$\vec{E} = \frac{1}{2} \{ \vec{E}^L \exp[i(k_L z - \omega_L t)] + \vec{E}^S \exp[i(k_S z - \omega_S t)] + \text{c.c.} \}, \quad (4)$$

$$\vec{P}^A = \frac{1}{2} \{ (\vec{P}^{L,\text{OA}} + \vec{P}^{L,\text{NL}}) \exp[i(k_L z - \omega_L t)] + (\vec{P}^{S,\text{OA}} + \vec{P}^{S,\text{NL}}) \exp[i(k_S z - \omega_S t)] + \text{c.c.} \}. \quad (5)$$

The superscripts OA and NL characterize terms leading to optical activity and stimulated Raman scattering, respectively. \vec{M}^A and \vec{Q}^A are written analogous to \vec{P}^A . The light beams propagate in the z direction. \vec{k} and ω are the wave vector and frequency of the light field, respectively. The subscripts and superscripts L and S stand for the laser and Raman Stokes fields, respectively. Neglecting second derivatives of the amplitudes with respect to space, we obtain the following for the amplitude of the Stokes field in the steady-state case:

$$\frac{d\vec{E}^S}{dz} = \frac{2\pi i \omega_S}{c_0 n_S} (\vec{P}_{\text{NL}}^S + \vec{P}_{\text{OA}}^S), \quad (6)$$

where

$$\vec{P}_e^S = \vec{P}^{S,e} - \frac{c_0}{\omega_S} (\vec{k}_S \times \vec{M}^{S,e}) - \frac{i}{6} \vec{k}_S \cdot \vec{Q}^{S,e}. \quad (7)$$

The effective polarizations \vec{P}_e^S leading to stimulated Raman scattering ($e = \text{NL}$) and optical activity ($e = \text{OA}$) are discussed below.

2. Optical activity

Optical activity has been treated on a molecular basis by Born,²¹ who obtained simple results for quartz. Different approaches to the phenomenological treatment of optical activity are discussed by Bokut' *et al.*²² In our calculations the terms in Eqs. (2) have been chosen in such a way to reproduce the simple results of Born's treatment.

We treat the special case of optical activity in α -quartz for light propagation in the z direction. We introduce the gyration tensor²¹ $\vec{\zeta}$ which has the same form as the dielectric tensor $\vec{\epsilon}$ of quartz, i.e., it has only diagonal elements $\zeta_{xx} = \zeta_{yy}$ and ζ_{zz} . The second-rank tensors $\vec{\zeta}^{A1}$ and $\vec{\zeta}^{A2}$ of Eqs. (2a) and (2b) are connected to the gyration tensor by²¹

$$\vec{\zeta}^{A1} = \frac{\vec{\zeta}}{k_S}, \quad (8)$$

$$\zeta_{ik}^{A2} = \frac{-\zeta_{ik}}{2k_S \epsilon_{kk}} = 0, \quad \text{for } i \neq k, \quad (9)$$

$$\zeta_{ii}^{A2} = \frac{\sum_j \zeta_{jj} - \zeta_{ii}}{2k_S \epsilon_{ii}}. \quad (10)$$

The third-rank tensor $\vec{\Lambda}$ of Eq. (2c) couples the electric quadrupole moment to the light field. It has the same form as the tensor \vec{A} which is responsible for Raman optical activity of the 468-cm⁻¹ mode of quartz (see Appendix).

The plane-wave approximation of Eqs. (4) and (5) is substituted in Eqs. (2). The effective polarization \vec{P}_{OA}^S is then given by

$$\vec{P}_{\text{OA}}^S = \frac{3i}{8\pi} \left[\zeta_{zz} + \frac{1}{3}\zeta_{xx} - \frac{4\pi}{9}k_S\Lambda_{xyz} \right] (\hat{k}_S \times \vec{E}^S), \quad (11)$$

where $\hat{k}_S = (0, 0, 1)$ is the unit vector in the z direction.

3. Nonlinear susceptibilities

The effective nonlinear polarization \vec{P}_{NL}^S has been treated in detail in Ref. 19. We shortly summarize the essential parts of the calculations.

It is convenient to fold the various contributions to the nonlinear susceptibilities $\vec{\chi}$ into a single effective susceptibility such that

$$\chi_{ijkl}^{\text{eff}} = \frac{N}{2hc_0\delta\bar{\nu}} [\alpha_{ij}\alpha_{kl} - i\alpha_{ij}(n_L G'_{i\rho}\delta_{\rho kz} - n_S G'_{k\rho}\delta_{\rho lz}) + i\alpha_{kl}(n_L G'_{i\rho}\delta_{\rho jz} - n_S G'_{j\rho}\delta_{\rho iz}) - \frac{1}{6}i\alpha_{ij}(k_L A_{lzk} - k_S A_{kzl}) + \frac{1}{6}i\alpha_{kl}(k_L A_{izj} - k_S A_{jzi})]. \quad (13)$$

δ_{ijk} is the fully antisymmetric Levi-Civita tensor.¹⁵ n_L and n_S are the refractive indices at the laser and Stokes frequency, respectively. N is the number density of primitive cells in the crystal, $\delta\bar{\nu}$ is the spontaneous Raman linewidth (in cm^{-1}), and h is Planck's constant. The electric dipole polarizability $\vec{\alpha}$ is responsible for Raman scattering. It can be seen from Eq. (13) that the interference terms between the electric dipole polarizability tensor $\vec{\alpha}$ and the magnetic dipole and electric quadrupole polarizability tensors \vec{G}' and \vec{A} lead to Raman optical activity. In the following sections the theory of SRS and Raman optical activity presented above is applied to the 132- and 468- cm^{-1} modes of α -quartz.

B. 132- cm^{-1} mode

1. Differential equations and solutions

The Raman scattering tensor $\vec{\alpha}$ of the 132- cm^{-1} E mode of α -quartz is given by^{3,23-25}

$$\vec{\alpha}(x) = \begin{pmatrix} c & 0 & 0 \\ 0 & -c & d \\ 0 & d & 0 \end{pmatrix}, \quad (14a)$$

$$\vec{\alpha}(y) = \begin{pmatrix} 0 & -c & -d \\ -c & 0 & 0 \\ -d & 0 & 0 \end{pmatrix}. \quad (14b)$$

The x direction corresponds to the a_1 axis of the quartz crystal. The y axis is orthogonal to the x and z direction. The magnetic dipole polarizability tensor \vec{G}' and the electric quadrupole polarizability tensor \vec{A} are given in the Appendix. For our calculations we need the tensor components

$$\vec{A}(x): A_{xzy} = A_{yzx} = A_d, A_{zxx} = A_{zyy} = 0, \quad (15a)$$

$$\vec{A}(y): A_{xzy} = A_{yzx} = 0, A_{zxx} = -A_{zyy} = A_d. \quad (15b)$$

$$P_{\text{NL},i}^S = \chi_{ijkl}^{\text{eff}} E_j^L E_k^{L*} E_l^S. \quad (12)$$

The nonlinear susceptibilities entering $\vec{\chi}^{\text{eff}}$ have been shown¹⁹ to be related to the matrix elements $\langle f | \vec{\alpha} | i \rangle$, $\langle f | \vec{G}' | i \rangle$, and $\langle f | \vec{A} | i \rangle$ of the electric dipole polarizability $\vec{\alpha}$, the magnetic dipole polarizability $\vec{G} = i\vec{G}'$, and the electric quadrupole polarizability \vec{A} , respectively. The matrix element $\langle f | \vec{\alpha} | i \rangle$ of the electric dipole polarizability tensor $\vec{\alpha}$ for the Raman transition between states i and f is termed the Raman scattering tensor. To simplify the notation we write, for the matrix element $\langle f | \vec{\alpha} | i \rangle$ of the electric dipole polarizability tensor with components $\langle f | \alpha_{ij} | i \rangle$, simply $\vec{\alpha}$ and α_{ij} , respectively. A similar notation is used for the other polarizability tensors. Using the relations given in Ref. 19, we get

The x and y components of \vec{G}' have the same form as those of $\vec{\alpha}$ (see Appendix).

We consider first stimulated Raman scattering in the forward direction and substitute Eqs. (11)–(15) in Eq. (6). The equations for the x and y components of the Stokes field E^S are given by

$$\frac{dE_x^S}{dz} = \frac{1}{2}\bar{g}_c \{ [|E^L|^2 + i\Delta_c^F (E_x^L E_y^{L*} - E_x^{L*} E_y^L)] E_x^S + (E_x^{L*} E_y^L - E_x^L E_y^{L*} + i\Delta_c^F |E^L|^2) E_y^S \} + \beta_S E_y^S, \quad (16)$$

$$\frac{dE_y^S}{dz} = \frac{1}{2}\bar{g}_c \{ (E_x^L E_y^{L*} - E_x^{L*} E_y^L - i\Delta_c^F |E^L|^2) E_x^S + [|E^L|^2 - i\Delta_c^F (E_x^{L*} E_y^L - E_x^L E_y^{L*})] E_y^S \} - \beta_S E_x^S. \quad (17)$$

The following abbreviations have been used: Raman gain factor

$$\bar{g}_c = (2\pi N \omega_S c^2) / (hc_0^2 n_S \delta\bar{\nu}_c), \quad (18)$$

specific rotatory power for the Stokes light

$$\beta_S = 3\omega_S \left[\zeta_{zz} + \frac{1}{3}\zeta_{xx} - \frac{4\pi}{9}k_S\Lambda_{xyz} \right] / (4n_S c_0), \quad (19)$$

which is positive for left-handed, optically active quartz,¹³ and the quantity

$$\Delta_c^F = -[6G'_c(n_L - n_S) + (k_L - k_S)A_d] / 3c, \quad (20)$$

which describes Raman optical activity for forward scattering. It will be shown in Sec. II B 3 that Δ_c^F is equal to the Raman circular intensity difference Δ_{spont} used in

spontaneous Raman scattering.¹⁶ For backward scattering we get

$$\Delta_c^B = -[6G_c'(n_L + n_S) + (k_L + k_S)A_d]/3c. \quad (21)$$

It is convenient to introduce left- and right-handed circularly-polarized light fields¹³

$$E_i^j = E_x^j + iE_y^j, \quad (22a)$$

$$E_r^j = E_x^j - iE_y^j, \quad (22b)$$

respectively ($j=L, S$). Equations (16) and (17) can then be written for forward Raman scattering in the simple form

$$\frac{dE_r^S}{dz} = \frac{1}{2}g_l^F I_l^L E_r^S + i\beta_S E_r^S, \quad (23)$$

$$\frac{dE_l^S}{dz} = \frac{1}{2}g_r^F I_r^L E_l^S - i\beta_S E_l^S. \quad (24)$$

I_r^L and I_l^L are the intensities of the right- and left-handed circularly-polarized components of the pump laser light. g_r^F and g_l^F are the corresponding forward Raman gain factors, which are given by

$$g_r^F = \frac{16\pi}{c_0 n_L} \bar{g}_c (1 + \Delta_c^F) = g_c (1 + \Delta_c^F), \quad (25)$$

$$g_l^F = g_c (1 - \Delta_c^F). \quad (26)$$

The Raman gain factor g_c is estimated in Sec. III C 1(b) to be about 3×10^{-3} cm/MW for $T \leq 10$ K. Its temperature dependence is given by the inverse spontaneous Raman linewidth $1/\delta\bar{\nu}_c$ [see Eq. (18)].

It is interesting to note that according to Eqs. (23) and (24) there is no coupling between the right- and left-handed Stokes components. For forward Raman scattering the right-circularly-polarized Stokes component E_r^S is amplified by the left-circularly-polarized laser intensity I_l^L and vice versa.

Equations (23) and (24) are solved and yield the forward scattered Stokes fields for a traveling-wave system of length l ,

$$E_r^S = E_r^S(0) \exp(\frac{1}{2}g_l^F I_l^L l + i\beta_S l), \quad (27)$$

$$E_l^S = E_l^S(0) \exp(\frac{1}{2}g_r^F I_r^L l - i\beta_S l). \quad (28)$$

$E_r^S(0)$ and $E_l^S(0)$ are the initial values of the Stokes fields. The x and y components of the Stokes field may be obtained from Eqs. (22), (27), and (28).

For elliptically polarized laser light, the forward Stokes intensity I^S for a traveling-wave system is obtained from Eqs. (27) and (28):

$$I^S = I_r^S(0) \exp(g_l^F I_l^L l) + I_l^S(0) \exp(g_r^F I_r^L l), \quad (29)$$

where $I_r^S(0)$ and $I_l^S(0)$ are the initial values of the Stokes intensities.

In our experiments elliptically polarized pump light is generated by a polarizer and a quarter-wave plate (see Sec. III A). The transmission direction of the polarizer and the optical axis of the quarter-wave plate form an angle γ . When I is the intensity of the incident light wave, the intensities of the right- and left-handed circularly-polarized components of the elliptically polarized pump wave can be

shown to be given by

$$I_r^L = \frac{1}{2}I(1 + \sin 2\gamma), \quad (30a)$$

$$I_l^L = \frac{1}{2}I(1 - \sin 2\gamma). \quad (30b)$$

In the following sections we derive an expression for the threshold intensity of SRS and discuss the polarization of the Stokes light.

2. Threshold intensity for stimulated Raman scattering

We define the threshold intensity I^{th} for stimulated Raman scattering as the laser intensity where the Raman Stokes signal I^S becomes detectable by our detection system. This corresponds to a Raman conversion efficiency of about 1%. The experimental detection limit I_D^S of the Stokes intensity and the laser intensities of Eq. (30) are substituted in Eq. (29). We get an equation for the determination of the threshold intensity I^{th} of SRS:

$$I_D^S = I_r^S(0) \exp[\frac{1}{2}g_l^F I^{\text{th}} l (1 - \sin 2\gamma)] + I_l^S(0) \exp[\frac{1}{2}g_r^F I^{\text{th}} l (1 + \sin 2\gamma)]. \quad (31)$$

The threshold intensity I^{th} is calculated numerically from Eq. (31).¹² If $g_r^F \neq g_l^F$, there is a difference in the threshold intensities of right- and left-circularly-polarized pump light ($\gamma = 45^\circ$ and 135° , respectively), which is due to Raman optical activity.

It is interesting to discuss approximate solutions of Eqs. (29) and (31). For $g_r^F I_r^L > g_l^F I_l^L$ the second term on the right-hand side of Eq. (29) dominates. Neglecting the first term, we find for the right-circularly-polarized component of the threshold intensity

$$I_r^{\text{th}} = \ln[I_D^S / I_l^S(0)] / g_r^F l. \quad (32)$$

From an estimate of the initial values of the Stokes intensity we calculate for the traveling-wave system a threshold gain of

$$G_r^{\text{th}} = g_r^F I_r^{\text{th}} l \simeq 30, \quad (33)$$

which is needed to exceed the detection limit I_D^S . With the use of Eq. (30a) the incident laser intensity at threshold as a function of γ is given by

$$I^{\text{th}}(\gamma) = \frac{2I_r^{\text{th}}}{1 + \sin 2\gamma}. \quad (34)$$

For $g_r^F I_r^L < g_l^F I_l^L$ an analogous expression may be derived.

Equations (18), (25), and (32) show that the threshold intensity I^{th} is proportional to the spontaneous Raman linewidth $\delta\bar{\nu}_c$, i.e., for a traveling-wave system the temperature dependence of I^{th} is the same as that of $\delta\bar{\nu}_c$.

3. Raman circular intensity difference

In spontaneous Raman scattering the Raman circular intensity difference Δ_{spont} was used to characterize Raman optical activity. It is defined by¹⁶ $\Delta_{\text{spont}} = (S_r - S_l) / (S_r + S_l)$, where S_r and S_l are the spontaneous Raman intensities for right- and left-circularly-polarized incident light, respectively. Both the spontaneous Raman intensity S and the Raman gain factor g are proportional to the Ra-

man scattering cross section.²⁰ For forward scattering the Raman circular intensity difference may therefore be written as

$$\Delta_{\text{spont}}^F = (g_r^F - g_l^F) / (g_r^F + g_l^F). \quad (35)$$

Using Eqs. (25) and (26) for g_r^F and g_l^F , we find $\Delta_{\text{spont}}^F = \Delta_c^F$. The Raman circular intensity difference may be determined from Raman gain measurements.¹⁹

For circularly-polarized pump light the Raman threshold intensity is given by I_r^{th} or I_l^{th} , which is proportional to $1/g_r$ or $1/g_l$, respectively [see, e.g., Eq. (32)]. With these relations Eq. (35) is written as

$$\Delta_{\text{spont}}^F = \Delta_c^F = (I_l^{\text{th}} - I_r^{\text{th}}) / (I_l^{\text{th}} + I_r^{\text{th}}). \quad (36)$$

This equation is also valid for backward scattering if superscript F is replaced by B and the Raman threshold intensity is measured in the backward direction. Application of Eq. (36) to experiments should be considered with caution, because in traveling-wave systems there is often a competition between forward and backward SRS, which has not been taken into account in the derivation of Eq. (36).

4. Polarization of the Raman Stokes light

The polarization of the Stokes light of stimulated Raman scattering in the traveling-wave system is discussed for different elliptical polarizations of the pump laser light with the use of Eqs. (27)–(30). As an example we consider the case where $g_r^F > g_l^F$, e.g., $g_r^F = 1.5g_l^F$. Four different situations are to be distinguished.

(i) The right-circularly-polarized component of the elliptically polarized pump light dominates, i.e., $g_r^F I_r^L > g_l^F I_l^L$. This condition is fulfilled when the angle γ between the electric field vector of the incident light and the optical axis of the quarter-wave plate which generates the elliptically polarized pump light (see Sec. III A) is in the range $0^\circ \leq \gamma \leq 90^\circ$ for $g_r^F = 1.5g_l^F$. The first term on the right-hand side of Eq. (29) is neglected. The Stokes light is left circularly polarized in a good approximation. It has the opposite sense of rotation as the elliptically polarized pump wave.

(ii) For $g_r^F I_r^L < g_l^F I_l^L$ ($100^\circ \lesssim \gamma \lesssim 170^\circ$) the left-circularly-polarized component of the pump light dominates, and the Raman light is right circularly polarized.

(iii) $g_r^F I_r^L \approx g_l^F I_l^L$ ($90^\circ \leq \gamma \leq 100^\circ$ and $170^\circ \leq \gamma \leq 180^\circ$). In these regions the Stokes light is elliptically polarized. The detailed Stokes polarization depends on the Raman gain factors and the laser polarization.

(iv) For $g_r^F I_r^L = g_l^F I_l^L$ ($\gamma \approx 95.8^\circ$ and 174.2° for $g_r^F = 1.5g_l^F$) the Raman light should be linearly polarized because the right- and left-handed Stokes components have equal amplitudes [see Eqs. (27) and (28)]. The orientation of the electric field vector of the Stokes wave depends on the optical rotatory power β_S .

5. Raman oscillator theory

(a) Frequency dependence of the Raman gain factor.

There is experimental evidence that the surfaces of the quartz crystal act as a resonator for the Stokes light [see

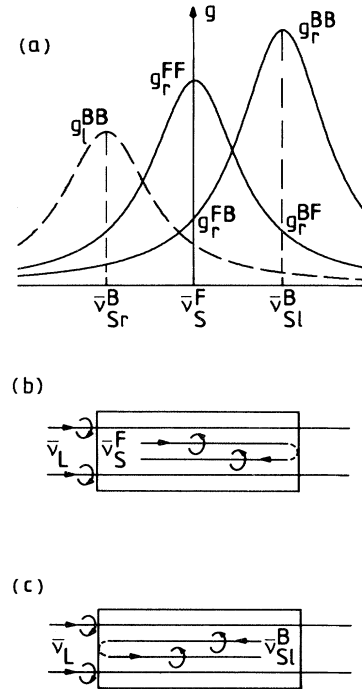


FIG. 1. (a) Gain profiles for forward and backward SRS of circularly polarized pump light. (b) and (c) Quartz crystal acting as a Raman resonator (for details see text).

Sec. III B 1(a)]. In the Raman oscillator forward and backward Raman scattering occur, which have different frequencies and gain factors for the 132-cm^{-1} mode because of the different wave vectors of the excited phonons. A linear wave-vector dependence of the frequency of the 132-cm^{-1} mode was found in Ref. 6. The mode is doubly degenerate for zero wave vector of the phonons, but the degeneracy is lifted to first order in wave vector along the c axis. The Raman spectrum of the 132-cm^{-1} mode shows at liquid-helium temperatures two closely spaced narrow lines which are circularly polarized with the opposite sense of rotation of the electric field vector.⁶ The line splitting increases linearly with the wave vector of the 132-cm^{-1} phonon. For a pump-laser wavelength of $1.064\ \mu\text{m}$ it is 6×10^{-4} and $0.083\ \text{cm}^{-1}$ for forward and backward scattering, respectively.⁶ The Raman linewidth of each component is $\delta\bar{\nu}_c = 0.05\ \text{cm}^{-1}$ for $T \leq 10\ \text{K}$.⁵

The frequency dependence of the Raman gain factor is determined by the shape of the spontaneous Raman line.²⁰ Therefore, the behavior of the Raman oscillator is strongly affected by the splitting of the 132-cm^{-1} Raman line. Figure 1(a) shows the frequency dependence of the Raman gain factor g for left- and right-circularly-polarized pump light as broken and solid lines, respectively. The Raman gain curves for both polarizations are clearly separated for backward scattering due to the frequency splitting of the Raman lines ($\bar{\nu}_{Sl}^B - \bar{\nu}_{Sr}^B = 8.3 \times 10^{-2}\ \text{cm}^{-1}$). The splitting $\bar{\nu}_{Sl}^F - \bar{\nu}_{Sr}^F = 6 \times 10^{-4}\ \text{cm}^{-1}$ for forward scattering is too small to be seen in Fig. 1(a), we assume $\bar{\nu}_{Sr}^F \approx \bar{\nu}_{Sl}^F = \bar{\nu}_S^F$. The peak values g_l^{BB} , g_r^{FF} , and g_r^{BB} of the gain factors of left-

and right-circularly-polarized pump light are different because Raman optical activity depends on the scattering direction [see Eqs. (20), (21), (25), and (26)]. It should be noted that subscript r (or l) of the gain factor refers to the *pump* light polarization. It corresponds to subscript l (or r) of the Stokes frequency, because laser and Stokes light have the opposite sense of rotation of the electric field vector for the 132-cm⁻¹ mode in quartz (see Sec. IIB 4). The first and second superscripts of g refer to the superscripts of the Stokes frequency $\bar{\nu}_S$ and the stimulated Raman circular intensity difference Δ_c , respectively. It will be discussed in Sec. IIIB 1(c) that in our experiments $\Delta_c^F \simeq 0$ and $\Delta_c^B \neq 0$, i.e., $g_r^{FF} \simeq g_l^{FF}$ and $g_r^{BB} \neq g_l^{BB}$.

(b) *Stimulated Raman Stokes intensity.* As an example we treat an oscillator pumped with right-circularly-polarized laser light. We consider first the case where the Raman oscillator starts with forward scattering [see Fig. 1(b)]. The Stokes light with frequency $\bar{\nu}_S^F$ is amplified with gain factor $g_r^{FF} = g_c(1 + \Delta_c^F)$, which corresponds to g_r^F of Eq. (25). After reflection at the end surface of the crystal, it is amplified at the wing of the backward scattering gain profile [see Fig. 1(a)] with gain factor

$$g_r^{FB} = g_r^{BB} / [1 + (\bar{\nu}_{Sl}^B - \bar{\nu}_S^F)^2 / (\delta\bar{\nu}_c / 2)^2], \quad (37)$$

where $g_r^{BB} = g_c(1 + \Delta_c^B)$. At the reflection, the polarization of circularly-polarized light is changed from left to right and vice versa. This is due to the change of propagation direction, while the sense of rotation of the electric field vector in a frame fixed in space remains unchanged at reflection.²⁶ The Raman gain depends on the relative sense of rotation of the laser and Stokes electric field vectors, which is not changed at reflection. Therefore, for backward Raman scattering the same laser and Stokes components interact with each other as for forward Raman scattering.

There is a second amplification process in the Raman oscillator [see Fig. 1(c)]. It starts with Raman backward scattering with frequency $\bar{\nu}_{Sl}^B$. The Stokes light is first

amplified with gain factor g_r^{BB} and after reflection with [see Fig. 1(a)]

$$g_r^{BF} = g_r^{FF} / [1 + (\bar{\nu}_{Sl}^B - \bar{\nu}_S^F)^2 / (\delta\bar{\nu}_c / 2)^2]. \quad (38)$$

We discuss now the iterative steps of the calculation of the left-circularly-polarized Stokes intensity $I_i^S(m)$ after m passages through the crystal with length l . After the first run we get for forward scattering with frequency $\bar{\nu}_S^F$ [Fig. 1(b)]

$$I_i^{SF}(1) = CI_r^L(1) \exp[g_r^{FF} I_r^L(1)l]$$

and for backward scattering with frequency $\bar{\nu}_{Sl}^B$ [Fig. 1(c)]

$$I_i^{SB}(1) = CI_r^L(1) \exp[g_r^{BB} I_r^L(1)l],$$

where $I_r^L(1)$ is the intensity of the right-circularly-polarized laser component at the first run through the crystal. We assumed the initial Stokes intensity for forward and backward scattering to be given by CI_r^L . The constant C is estimated from spontaneous Raman data. After the second run we get for the forward Stokes intensity

$$I_i^{SF}(2) = CI_r^L(2) \exp[g_r^{FF} I_r^L(2)l] + RI_i^{SB}(1) \exp[g_r^{BF} I_r^L(2)l], \quad (39a)$$

where the second term on the right-hand side represents the amplified reflected backward Stokes intensity of the first run. R is the reflectivity of the quartz surfaces. The backward Stokes intensity is given by

$$I_i^{SB}(2) = CI_r^L(2) \exp[g_r^{BB} I_r^L(2)l] + RI_i^{SF}(1) \exp[g_r^{FB} I_r^L(2)l]. \quad (39b)$$

In the third run we take into account that the first and second terms on the right-hand side of Eq. (39b) have different frequencies $\bar{\nu}_{Sl}^B$ and $\bar{\nu}_S^F$, respectively. After reflection they are amplified therefore with different gain factors. The forward Stokes intensity is given by

$$I_i^{SF}(3) = CI_r^L(3) \exp[g_r^{FF} I_r^L(3)l] + RCI_r^L(2) \exp[g_r^{BB} I_r^L(2)l] + g_r^{BF} I_r^L(3)l + R^2 I_i^{SF}(1) \exp[g_r^{FB} I_r^L(2)l] + g_r^{FF} I_r^L(3)l.$$

An equivalent expression is obtained for the backward direction. After m passages through the crystal we get for the forward Stokes intensity outside the crystal (m even)

$$I_i^{SF}(m) = (1-R)C \left\{ \exp[g_r^{FF} I_r^L(m)l] \left[I_r^L(m) + \sum_{\nu=1}^{m/2-1} I_r^L(m-2\nu) R^{2\nu} \exp \left[l \sum_{\mu=m/2-\nu}^{m/2-1} [g_r^{FF} I_r^L(2\mu) + g_r^{FB} I_r^L(2\mu+1)] \right] \right] \right. \\ \left. + \sum_{\nu=0}^{m/2-1} I_r^L(m-2\nu-1) R^{2\nu+1} \exp \left[l \sum_{\mu=m/2-\nu}^{m/2} [g_r^{BB} I_r^L(2\mu-1) + g_r^{BF} I_r^L(2\mu)] \right] \right\}. \quad (40)$$

Mode-pulling effects are neglected in Eq. (40).

An expression similar to Eq. (40) can be derived for right-circularly-polarized Stokes light, leaving the Raman oscillator in the forward direction. When the laser light is elliptically polarized, the total intensity is given by $I^S = I_r^S + I_l^S$.

(c) *Threshold intensity for stimulated Raman scattering.* We discuss the dependence of the threshold intensity I^{th} on pump-laser polarization, which is varied by changing

the angle γ between the electric field vector of the laser light and the optical axis of a quarter-wave plate (see Sec. IIIA). We consider first the region of laser polarization, i.e., of γ , where $I_r^S \ll I_l^S$. It can be seen from Eq. (33) that an amplification of the Stokes light of about e^{30} is necessary to exceed the experimental detection limit I_D^S . This amplification is reached in Eq. (40) when the right-circularly-polarized component I_r^L of the pump light exceeds the threshold value I_r^{th} . Using Eq. (30), we find

the threshold intensity of the incident laser light

$$I^{\text{th}}(\gamma) = \frac{2I_r^{\text{th}}}{1 + \sin 2\gamma}. \quad (41a)$$

In the region of γ where I_r^S dominates, we get

$$I^{\text{th}}(\gamma) = \frac{2I_l^{\text{th}}}{1 - \sin 2\gamma}. \quad (41b)$$

It is interesting to note that the dependence of the threshold intensity on pump polarization is the same for the Raman oscillator and the traveling-wave system [see, e.g., Eq. (34)] over almost the complete range of γ . The absolute values of the threshold intensities I_r^{th} , I_l^{th} , and I^{th} differ substantially for the oscillator and traveling-wave system.

For the calculation of the absolute values of the Raman threshold we use a gain factor of $g_c = 3 \times 10^{-3}$ cm/MW [see Sec. III C 1(b)] and a crystal length of $l = 8$ cm. It will be shown in Sec. III B 1(c) that agreement with experiments is obtained with Raman circular intensity differences $\Delta_c^F = 0$ and $\Delta_c^B = 0.48$. In the oscillator calculations we use a Gaussian time dependence of the pump-laser pulse with a $1/e$ half-width of 11 ns and a reflectivity of the quartz surfaces of $R = 0.04$. With the numbers given above we find threshold intensities for right-circularly-polarized pump light of 833 and 212 MW/cm² for the traveling-wave system and the oscillator system [Eq. (40)], respectively. Owing to the feedback from the crystal surfaces, the threshold intensity of the oscillator system is substantially lower than for the traveling-wave system.

The temperature dependence of the Raman oscillator threshold intensity is more complicated than for the traveling-wave system. There are two counteracting effects. (i) The gain factors g_r^{FF} and g_r^{BB} decrease with increasing temperature because of the increasing Raman linewidth⁵ $\delta\bar{\nu}_c$ [see Eqs. (18) and (25)]. This effect is the same as in the traveling-wave system. (ii) For the gain factors g_r^{FB} and g_r^{BF} the decrease of g_r^{BB} and g_r^{FF} with T is compensated by the increase of the Lorentz factors in Eqs. (37) and (38). As a result the threshold intensity for the oscillator system rises less with temperature than for the traveling-wave system. The results of quantitative calculations using the numbers given above and the Raman linewidth from Ref. 5 are shown in Fig. 5.

The polarization properties of the Raman Stokes light for the oscillator system are similar to the traveling-wave system (see Sec. II B 4).

C. 468-cm⁻¹ mode

1. Differential equations and solutions

The Raman scattering tensor of the 468-cm⁻¹ A_1 mode is given by^{3,23-25}

$$\vec{\alpha} = \begin{pmatrix} a & 0 & 0 \\ 0 & a & 0 \\ 0 & 0 & b \end{pmatrix}. \quad (42)$$

The magnetic dipole polarizability tensor $\vec{\vec{G}}'$ and the electric quadrupole polarizability tensor $\vec{\vec{A}}$ are given in the

Appendix. Tensor $\vec{\vec{G}}'$ is obtained from (42) by replacing a and b by G'_a and G'_b , respectively. For our calculations we need the following tensor components of $\vec{\vec{A}}$:

$$A_{xzy} = -A_{yzx} = A_b$$

and

$$A_{xxx} = A_{yyz} = 0.$$

(43)

We substitute Eqs. (11)–(13), (42), and (43) in Eq. (6) and get differential equations for the x and y components of the Stokes field for the traveling-wave case:

$$\begin{aligned} \frac{dE_x^S}{dz} = & \frac{1}{2}\bar{g}_a \{ [|E_x^L|^2 + i\Delta_a^F (E_x^L E_y^{L*} - E_x^{L*} E_y^L)] E_x^S \\ & + (E_x^L E_y^{L*} - i\Delta_a^F |E^L|^2) E_y^S \} + \beta_S E_y^S, \end{aligned} \quad (44)$$

$$\begin{aligned} \frac{dE_y^S}{dz} = & \frac{1}{2}\bar{g}_a \{ (E_x^{L*} E_y^L + i\Delta_a^F |E^L|^2) E_x^S \\ & + [|E_y^L|^2 + i\Delta_a^F (E_x^L E_y^{L*} - E_x^{L*} E_y^L)] E_y^S \} \\ & - \beta_S E_x^S. \end{aligned} \quad (45)$$

The Raman gain factor of the 468-cm⁻¹ mode is

$$\bar{g}_a = \frac{c_0 n_L}{8\pi} g_a = \frac{2\pi N \omega_S}{hc_0^2 n_S \delta\bar{\nu}_a} a^2. \quad (46)$$

The Raman optical activity for forward and backward Raman scattering is characterized by

$$\Delta_a^F = -[6G'_a(n_L + n_S) + (k_L + k_S)A_b]/6a, \quad (47a)$$

$$\Delta_a^B = -[6G'_a(n_L - n_S) + (k_L - k_S)A_b]/6a, \quad (47b)$$

respectively.

The differential equations for the right- and left-circularly-polarized components of the Stokes field are obtained from Eqs. (22), (44), and (45). We have

$$\frac{dE_r^S}{dz} = \frac{1}{4}\bar{g}_a [(1 + 2\Delta_a^F) |E_r^L|^2 E_r^S + E_r^L E_l^{L*} E_l^S] + i\beta_S E_r^S, \quad (48)$$

$$\frac{dE_l^S}{dz} = \frac{1}{4}\bar{g}_a [E_l^L E_r^{L*} E_r^S + (1 - 2\Delta_a^F) |E_l^L|^2 E_l^S] - i\beta_S E_l^S. \quad (49)$$

We take into account optical activity of the quartz crystal by substituting the following for the light fields in Eqs. (48) and (49):

$$E_r^j = \bar{E}_r^j \exp(i\beta_j z), \quad (50a)$$

$$E_l^j = \bar{E}_l^j \exp(-i\beta_j z) \quad (j = L, S). \quad (50b)$$

Equation (49) is then differentiated with respect to z . In the resulting equation the Stokes field \bar{E}_r^S and the derivative $d\bar{E}_r^S/dz$ are expressed by \bar{E}_l^S with the use of Eqs. (49) and (48), respectively. We get a second-order differential equation for \bar{E}_l^S :

$$\frac{d^2 \bar{E}_i^S}{dz^2} - \left[\frac{1}{2} \bar{g}_a |E^L|^2 \left(1 + \Delta_a^F \frac{|E_r^L|^2 - |E_i^L|^2}{|E^L|^2} \right) - 2i(\beta_L - \beta_S) \right] \frac{d \bar{E}_i^S}{dz} - \frac{1}{2} \left[\frac{1}{2} (\bar{g}_a \Delta_a^F)^2 |E_r^L|^2 |E_i^L|^2 + i(\beta_L - \beta_S) \bar{g}_a |E_i^L|^2 (1 - 2\Delta_a^F) \right] \bar{E}_i^S = 0. \quad (51)$$

Equation (51) is solved by the ansatz

$$\bar{E}_i^S = C_1 \exp(r_1 z) + C_2 \exp(r_2 z). \quad (52)$$

The expressions for r_1 and r_2 are not given here because they are too lengthy and a simple approximation is found for our experimental situation. The difference $\beta_L - \beta_S$ between the optical rotatory powers at the laser and Stokes frequency is about 0.18 rad/cm.²⁷ The Raman gain factor has been estimated in Sec. III C 1(b) to be $g_a = (1.1 \pm 0.4) \times 10^{-3}$ cm/MW for $\lambda_L = 1.064 \mu\text{m}$ at $T \leq 70$ K. It will be shown in Sec. III C 1(a) that the threshold intensity I^{th} for the 468-cm⁻¹ mode is about 1.4 GW/cm², i.e., $g_a I^L \geq 1.5 \text{ cm}^{-1}$, and nearly independent of pump-laser polarization. From these results it follows that $\beta_L - \beta_S \ll g_a I^L$ and $\Delta_a(I_r^L - I_i^L)/I^L \ll 1$. Using these approximations, we get from Eqs. (51) and (52)

$$r_1 = \frac{1}{2} g_a I^L \left[1 - 16 \left(\frac{\beta_L - \beta_S}{g_a I^L} \right)^2 \frac{I_r^L I_i^L}{(I^L)^2} + 2 \Delta_a^F \frac{I_r^L - I_i^L}{I^L} \right] - 2i(\beta_L - \beta_S) \frac{I_r^L}{I^L}, \quad (53)$$

$$r_2 = 8 g_a I^L \left(\frac{\beta_L - \beta_S}{g_a I^L} \right)^2 \frac{I_r^L I_i^L}{(I^L)^2} - 2i(\beta_L - \beta_S) \frac{I_i^L}{I^L}. \quad (54)$$

The right-circularly-polarized Stokes component \bar{E}_r^S is calculated from Eqs. (49) and (52). With the use of the results for E_r^S and E_i^S , the constants C_1 and C_2 are determined as a function of the initial conditions $E_r^S(0)$ and $E_i^S(0)$ for the Stokes light. The Raman gain for the Stokes light field corresponds to the real parts of r_1 and r_2 . For $(\beta_L - \beta_S)/g_a I^L \ll 1$ we find $\text{Re}\{r_1\} \gg \text{Re}\{r_2\}$ and obtain the following for the Stokes fields of a traveling-wave system with length l :

$$E_i^S = \{ [|E_i^L|^2 E_i^S(0) + E_i^L E_r^{L*} E_r^S(0)] / (2 |E^L|^2) \} \times \exp(r_1 l - i\beta_S l), \quad (55)$$

$$E_r^S = E_i^S E_r^L / E_i^L. \quad (56)$$

We calculate the total Stokes intensity $I^S = I_r^S + I_i^S$ from Eqs. (55) and (56). Neglecting the second term in the square brackets of Eq. (53), we get

$$I^S = I^S(0) \exp\{ g_a I^L [1 + 2\Delta_a^F (I_r^L - I_i^L) / I^L] l \}, \quad (57)$$

where $I^S(0)$ is an effective initial value that may be calculated from the square bracket of Eq. (55).

2. Threshold intensity for stimulated Raman scattering

The threshold intensity I^{th} for SRS is obtained from Eq. (57) by equating the Stokes intensity to the experimental detection limit I_D^S . Neglecting Raman optical activity ($\Delta_a^F = 0$) we get

$$I^{\text{th}} = \ln[I_D^S / I^S(0)] / (g_a l). \quad (58)$$

The only term in Eq. (58) which depends on the pump-laser polarization is the effective initial value $I^S(0)$. However, this dependence may be neglected because $I^S(0)$ enters via the logarithmic term in Eq. (58). For negligible Raman optical activity we expect the threshold intensity

for SRS from the 468-cm⁻¹ mode to be independent of the pump-laser polarization. This behavior is in contrast to the threshold intensity dependence of the 132-cm⁻¹ mode. The difference between both modes is due to their different symmetry.

3. Polarization of the Raman Stokes light

For a discussion of the polarization properties a few fundamental relations of polarization optics should be recalled. The magnitudes E_ξ and E_η of the principal axes of elliptically polarized light are determined by the amplitudes of the right- and left-circularly-polarized components²⁸

$$E_\xi^j = \frac{1}{2} (|E_i^j| + |E_r^j|), \quad (59a)$$

$$E_\eta^j = \frac{1}{2} (|E_i^j| - |E_r^j|) \quad (j = L, S). \quad (59b)$$

The orientation of the axes is obtained from the phase difference of the right- and left-circularly-polarized fields. Using Eqs. (55), (56), and (59), we calculate the major and minor axes of the ellipse of the Raman Stokes light

$$E_\xi^S = E_\xi^L |E_i^S| / |E_i^L|, \quad (60a)$$

$$E_\eta^S = E_\eta^L |E_i^S| / |E_i^L|. \quad (60b)$$

It follows immediately from Eqs. (60) that the ratios of major to minor axis of the ellipse of Stokes and laser light are equal, i.e.,

$$E_\xi^S / E_\eta^S = E_\xi^L / E_\eta^L. \quad (61)$$

The principal axes of the ellipses of Stokes and laser light have, in general, different orientations depending on the values of the optical rotatory powers β_L and β_S .

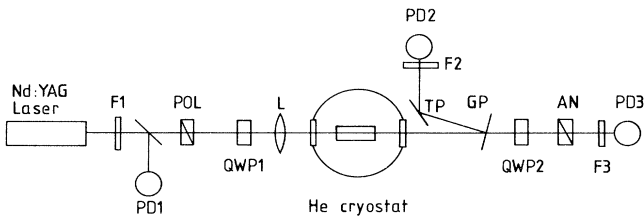


FIG. 2. Experimental setup for the investigation of SRS from the 132- and 468-cm⁻¹ modes of α -quartz. F1, F2, and F3—filters; PD1, PD2, and PD3—photodiodes; POL and AN—polarizers; QWP1 and QWP2—quarter-wave plates; L—lens; GP—glass plate; and TP—90° deflecting prism.

4. Raman oscillator theory

The oscillator theory for the 468-cm⁻¹ mode is simpler than for the 132-cm⁻¹ mode because there is no shift and splitting of the spontaneous Raman line. We neglect Raman optical activity, i.e., we assume $\Delta_a^F \approx \Delta_a^B \approx 0$ [Eqs. (47)], since the experimental results of Sec. III C 1(a) provide no evidence of Raman optical activity within the experimental accuracy. In this case the four gain factors g_a^{FF} , g_a^{FB} , g_a^{BF} , and g_a^{BB} are equal. We expect the same dependence of the threshold intensity I^{th} on pump polarization and temperature for the oscillator and traveling-wave theory. The absolute value of I^{th} , however, is lower for the oscillator system than for the traveling-wave system.

III. EXPERIMENTAL RESULTS AND DISCUSSION

A. Experimental setup

Stimulated Raman scattering in quartz is excited by a Nd:YAG (yttrium-aluminum-garnet) laser system, emitting single longitudinal- and transverse-mode light pulses with a duration of about 18 ns and an energy of 30 mJ. The frequency width of the Nd:YAG laser line is about 0.005 cm⁻¹. It is small compared to the spontaneous Raman linewidth of 0.05 cm⁻¹ of the 132-cm⁻¹ mode at liquid-helium temperature.⁵ The laser power is attenuated by filters F1 and registered by a fast photodiode PD1 (see Fig. 2). The pump-light polarization is adjusted by polarizer POL and quarter-wave plate QWP1. The polarization is varied by rotating the optical axis of the quarter-wave plate. The laser light is focused with lens L (focal length 80 cm) into the quartz crystal (length $l=8$ cm, diameter $d=1$ cm). The entrance and exit surfaces of the quartz crystal are perpendicular to the optical axis (c axis) within 0.5°. The laser light propagates along the c axis. Two quartz crystals were used whose end surfaces were nearly parallel with an angle of $\theta \approx 10''$ and $\theta \approx 1'$. The end surfaces of the crystal form a Raman resonator with a reflectivity of $R=0.04$. Since the Raman threshold is small at low temperatures,³ the crystal is mounted on a

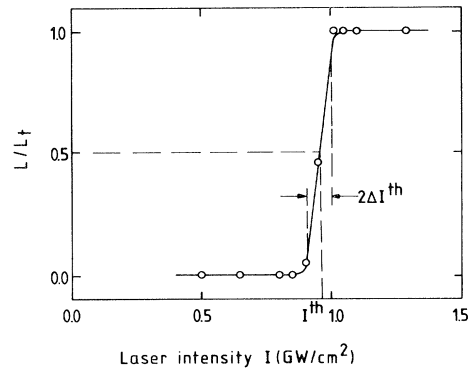


FIG. 3. Ratio of the number L of laser pulses with SRS to the total number L_t of laser pulses vs incident laser intensity I . I^{th} threshold laser intensity; ΔI^{th} error limit.

cold finger in the vacuum chamber of a helium cryostat. The temperature of the quartz crystal was varied between 10 and 70 K.

The Raman Stokes light is measured with photodiodes PD2 and PD3. The transmitted laser light is discriminated by filters F2 and F3. The polarization of the Raman Stokes light is analyzed by the quarter-wave plate QWP2 and the analyzer AN (see Fig. 2) as described in Ref. 21. The direction of the optical axis of QWP2 and the transmission direction of analyzer AN are varied independently to find the positions where extinction is obtained with the analyzer. In this case the optical axis of QWP2 is parallel to one of the principal axes of the ellipse of the Stokes light. The ratio of major to minor axes and the phase shift between y and x component of the Stokes field are calculated from the orientations of QWP2 and AN according to Ref. 21. Part of the Raman pulse is coupled out for reference by glass plate GP and is directed to photodiode PD2 via a 90° deflection prism TP. Glass plate GP is inserted nearly normal to the laser path to minimize changes of the Stokes polarization.

The pump-laser threshold intensity for stimulated Raman scattering is determined in the following way. The pump-laser power is measured by the calibrated photodiode PD1 and the corresponding Stokes power is recorded with photodiode PD3. A detectable signal at photodiode PD3 corresponds to a Raman conversion efficiency of about 1%. The pump-laser intensity I is calculated from the pump power and the measured laser beam area. Photodiodes PD1 and PD3 are interfaced to a computer. The ratio of laser pulses L with detectable Stokes signal to the total number L_t of laser pulses is plotted versus pump-laser intensity I in Fig. 3.

The threshold intensity I^{th} for SRS is defined by $L/L_t=0.5$. The error limits ΔI^{th} of our experimental results correspond to $L/L_t=0.1$ and 0.9 (see Fig. 3). The relative error $\Delta I^{\text{th}}/I^{\text{th}}$ of the threshold intensity is typically 5%. For each determination of the threshold intensity at a definite pump-laser polarization about 200 laser shots are analyzed by the computer.

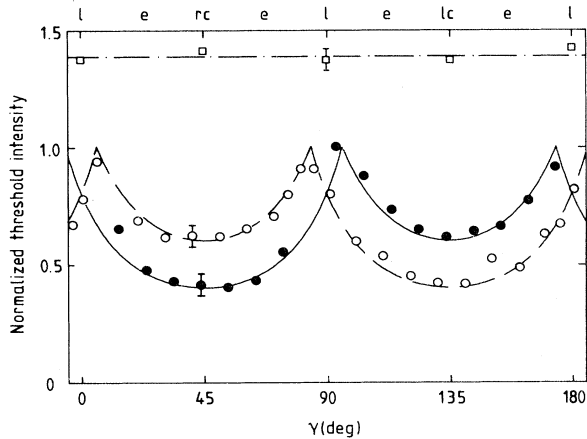


FIG. 4. Normalized threshold intensity $I^{\text{th}}(\gamma)/[I^{\text{th}}(45^\circ) + I^{\text{th}}(135^\circ)]_{132\text{ cm}^{-1}}$ of SRS vs angle γ . The open and solid circles correspond to the 132-cm^{-1} mode of right- and left-handed, optically active quartz, respectively. The open rectangles represent the 468-cm^{-1} mode. The solid, broken, and dashed-dotted lines are calculated curves. *l* linearly, *e* elliptically, *rc* right circularly, and *lc* left circularly polarized pump light.

B. 132-cm^{-1} mode

1. Threshold intensity for stimulated Raman scattering

(a) *Quartz crystals with different angles between the end surfaces.* Two quartz crystals with different angles θ between the end surfaces were investigated at $T = 10\text{ K}$. For right-circularly-polarized pump light the threshold intensity of the crystal with $\theta \approx 10''$ was lower by about a factor of 1.8 than that with $\theta \approx 1'$. In addition the threshold intensity increased with rising angle between the laser beam and the optical axis of the quartz crystal. Both results indicate that the surfaces of the crystal form a Raman resonator. The measured threshold intensity for right-circularly-polarized pump light is about 400 MW/cm^2 (for $\theta \approx 10''$). In Sec. III C 1(b) the Raman gain factor g_c of the 132-cm^{-1} mode is determined by comparison of the threshold intensity of this mode with the 468-cm^{-1} mode, whose gain factor is taken from spontaneous Raman data. Using this value of $g_c = (3 \pm 2) \times 10^{-3}\text{ cm/MW}$ we calculated in Sec. II B 5(c) threshold intensities of 212 and 833 MW/cm^2 for the oscillator system and the traveling-wave system, respectively. The measured threshold intensity of about 400 MW/cm^2 is between the two limiting cases. This fact indicates that an oscillator with a reduced number of passages through the crystal due to the angle θ between the crystal surfaces gives the best description of the experimental situation.

(b) *Dependence on pump-laser polarization.* The threshold intensity for SRS was measured for different polarizations of the pump laser light at $T \approx 10\text{ K}$. The pump-light polarization was varied by changing the angle γ of the optical axis of the quarter-wave plate QWP1 with respect to the transmission direction of polarizer POL (see Fig. 2).

The measured threshold intensities $I^{\text{th}}(\gamma)$ are normalized to the sum $I^{\text{th}}(45^\circ) + I^{\text{th}}(135^\circ)$, which is of the order of 1 GW/cm^2 . The results are plotted in Fig. 4. The open and solid circles correspond to SRS from the 132-cm^{-1} mode of right- and left-handed, optically active quartz crystals,¹³ respectively. The solid and broken lines are calculated according to Eqs. (40) and (41) of the oscillator theory. It should be mentioned, however, that the polarization dependence of the threshold intensity is the same for the traveling-wave and oscillator systems over almost the complete range of γ . There is good agreement between theory and experiments. The following results should be emphasized. (i) The Raman threshold is lowest for circularly-polarized pump light ($\gamma = 45^\circ$ and 135°). (ii) There is a difference in threshold intensities for right- and left-handed circularly-polarized pump light, which has the opposite sign for right- and left-handed, optically active quartz crystals.¹³ It is caused by Raman optical activity. Neglecting Raman optical activity, the Raman threshold intensities for right- and left-circularly-polarized pump light must be equal [see Eqs. (25), (26), and (31)].

(c) *Raman circular intensity difference.* We determine the Raman circular intensity difference Δ_c^F and Δ_c^B for forward and backward scattering by comparing the measured ratio $I^{\text{th}}(135^\circ)/I^{\text{th}}(45^\circ)$ of the threshold intensities of left- and right-circularly-polarized light with calculations. Since the end surfaces of the quartz crystal form a Raman resonator [see Sec. III B 1(a)], comparison is made with the Raman oscillator theory of Sec. II B 5. According to Eq. (20) the forward Raman circular intensity difference Δ_c^F is determined by the differences of the refractive indices, $n_L - n_S$, and wave vectors, $k_L - k_S$, while the sums of these quantities enter Δ_c^B for backward scattering [see Eq. (21)]. We expect, therefore, Raman optical activity in the backward direction to be large compared to the forward direction, i.e., $\Delta_c^B \gg \Delta_c^F$. In the calculations we assume Δ_c^F to be zero. The measured ratio $I^{\text{th}}(135^\circ)/I^{\text{th}}(45^\circ) = 1.5$ (for left-handed, optically active quartz) is reproduced by the oscillator calculations when a value of $\Delta_c^B = 0.48$ is used.

In Ref. 12 the results of Fig. 4 were discussed using a traveling-wave theory, i.e., neglecting the effect of reflections on the Raman intensity. Since the difference between forward and backward scattering was also not taken into account, a mean value of $(\Delta_c)_{\text{av}} \approx 0.2$ was determined from the experimental results.¹²

The measured value of Δ_c^B of quartz is considerably larger than the Raman circular intensity differences Δ_{spont} of chiral molecules investigated recently.^{14,15} The origin of this large difference is not clear at present.

(d) *Polarizability tensors.* The magnetic dipole polarizability G'_c and the electric quadrupole polarizability A_d may be determined from the Raman circular intensity differences Δ_c^F and Δ_c^B using Eqs. (20) and (21). However, the small value of Δ_c^F cannot be calculated with sufficient accuracy from our experimental results. We therefore use the results of spontaneous Raman measurements⁶ to determine G'_c and A_d . Pine and Dresselhaus⁶ investigated spontaneous Raman scattering in the backward direction from the 132-cm^{-1} mode in quartz at liquid-helium temperature. For a laser wavelength of $\lambda_L = 488\text{ nm}$ they

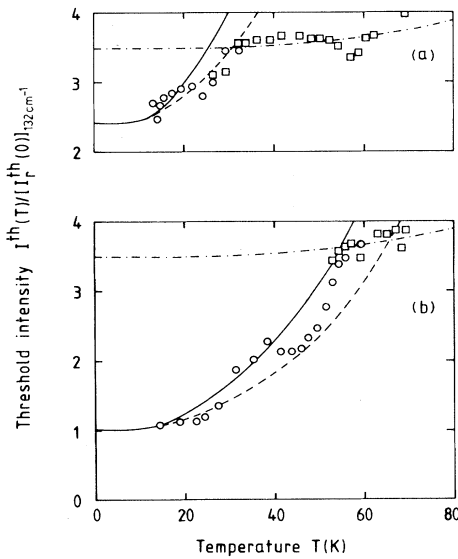


FIG. 5. Normalized threshold intensity $I^{\text{th}}(T)/[I_r^{\text{th}}(0)]_{132\text{ cm}^{-1}}$ of SRS in α -quartz vs temperature T . The open circles and rectangles correspond to the 132- and 468- cm^{-1} modes, respectively. The solid, broken, and dashed-dotted lines are calculated curves (for details see text). (a) Linearly polarized pump light. (b) Right-circularly-polarized pump light.

found no difference in the spontaneous Raman intensities of right- and left-circularly-polarized incident light. We conclude that $\Delta_c^B(488\text{ nm}) \simeq 0$. Spontaneous Raman measurements were also made at a laser wavelength of $\lambda_L = 632.8\text{ nm}$. For this wavelength a small difference in the Raman intensities of right- and left-circularly-polarized incident light was found. We estimate a value of $\Delta_c^B(632.8\text{ nm})$ of about 0.08 from Fig. 4 (upper trace) of Ref. 6. Together with $\Delta_c^B(488\text{ nm}) \simeq 0$ we get $|G'_c|/c = 0.06 \pm 0.03$ and $|A_d|/c = (3.01 \pm 1.5) \times 10^{-6}\text{ cm}$. The Raman scattering tensor component c is estimated from the gain factor g_c to be about $3.6 \times 10^{-26}\text{ cm}^3$ [Eqs. (18) and (25)].

(e) *Temperature dependence.* We measured the threshold intensity I^{th} of SRS as a function of temperature for right-circularly, left-circularly, and linearly polarized pump light in left-handed optically active quartz. In Figs. 5(a) and 5(b) the threshold intensity is plotted versus temperature T for linearly and right-circularly-polarized pump light, respectively. The solid and broken lines correspond to the traveling-wave and oscillator systems, respectively. The curves are fitted to the experimental points. All threshold intensities are normalized to the threshold intensity $[I_r^{\text{th}}(0)]_{132\text{ cm}^{-1}}$ of the 132- cm^{-1} mode for $T \rightarrow 0\text{ K}$. The circles and rectangles correspond to the 132 and 468- cm^{-1} modes, respectively. The 468- cm^{-1} mode will be discussed below [Sec. III C 1(b)].

In Fig. 5(b) the threshold intensity I_r^{th} of the 132- cm^{-1} mode increases drastically with rising temperature. It follows from Eqs. (18) and (32) that in a traveling-wave sys-

tem the threshold intensity is proportional to the spontaneous Raman linewidth $\delta\bar{\nu}_c$, which has been measured⁵ as a function of T . In Ref. 5 the experimental results were discussed using phonon decay and scattering processes and were found to be in good agreement with calculations. The normalized Raman linewidth $\delta\bar{\nu}_c(T)/\delta\bar{\nu}_c(0)$ is shown as a solid line in Fig. 5(b). The broken line is calculated according to the Raman oscillator theory of Sec. II B 5(c). The increase of I^{th} is smaller for the oscillator system than for the traveling-wave system. In the oscillator system the gain factors g_r^{FF} and g_r^{FB} of the forward and backward propagating Stokes light are different due to the different center frequencies of the Raman gain profiles [see Fig. 1(a)]. This difference decreases with increasing temperature because of the increasing Raman linewidth.⁵ Thus the increase of I^{th} with $\delta\bar{\nu}_c$ in the traveling-wave system is partially compensated by the larger values of g_r^{FB} and g_r^{BF} [see Eqs. (37) and (38)] in the oscillator system for higher temperatures.

In Fig. 5(a) the results for linearly polarized pump light are shown. The discussion is similar to Fig. 5(b). The only difference between both figures is the higher threshold intensity of the 132- cm^{-1} mode for linearly polarized laser light compared to right-circularly-polarized laser light.

2. Polarization of the Raman Stokes light

The polarization of the stimulated Raman Stokes light was determined for different polarizations of the pump-laser light. It was analyzed with quarter-wave plate QWP2 and analyzer AN according to the procedure described in Sec. III A. The measurements were carried out at $T = 20\text{ K}$ for left-handed optically active quartz. In Fig. 6 the ratios of the minor to major axes E_{mi}/E_{ma} of the laser and Stokes ellipses (triangles and circles, respectively) are plotted versus angle γ between the transmission direction of polarizer POL and the optical axis of quarter-wave plate QWP1. The open and solid symbols correspond to right- and left-handed polarized light.¹³ Three different regions are distinguished.

(i) For $0^\circ \leq \gamma \leq 87^\circ$ the ratio E_{mi}^S/E_{ma}^S is about 1 within the experimental accuracy. The Stokes light is left circularly polarized. It has the opposite sense of rotation of the electric field vector as the elliptically polarized laser light.

(ii) For $104^\circ \leq \gamma \leq 166^\circ$ the laser light has left-handed elliptical polarization, while the Stokes light is right circularly polarized.

(iii) In the regions $87^\circ \leq \gamma \leq 104^\circ$ and $166^\circ \leq \gamma \leq 180^\circ$ measurements of the Stokes polarization were difficult because of the large fluctuations of the Raman light.

The experimental results of regions (i) and (ii) are in agreement with the calculations of Secs. II B 4 and II B 5.

C. 468- cm^{-1} mode

1. Raman threshold intensities

(a) *Dependence on pump-laser polarization.* Stimulated Raman scattering from the 468- cm^{-1} mode of α -quartz

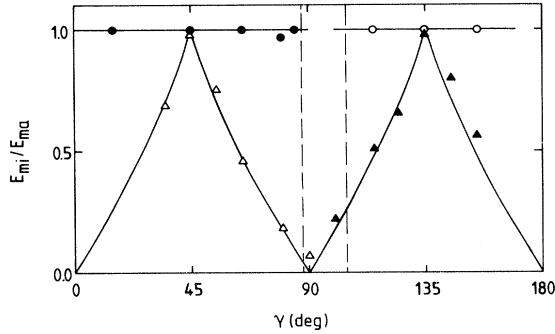


FIG. 6. Ratio E_{mi}/E_{ma} of minor to major axes of the ellipses of the laser and stimulated Stokes light of the 132-cm^{-1} mode vs angle γ . The triangles and circles correspond to the laser and Stokes light, respectively. The open symbols represent right-handed polarization, the solid symbols left-handed polarization.

was investigated at $T=65$ K. The dependence of the Raman threshold intensity on pump-laser polarization is shown in Fig. 4. The threshold intensity (\square) is normalized to the sum $[I_r^{\text{th}}(45^\circ) + I_r^{\text{th}}(135^\circ)]_{132\text{ cm}^{-1}}$ of the threshold intensities of the 132-cm^{-1} mode and plotted versus angle γ of the polarizer POL, with respect to the optical axis of quarter-wave plate QWP1. The threshold intensity is about 1.4 GW/cm^2 . Within the experimental accuracy it is independent of pump-laser polarization. This result is expected from Eqs. (57) and (58) if effects of Raman optical activity are neglected. We conclude that the Raman circular intensity differences are small, i.e., Δ_a^F and $\Delta_a^B \ll 1$.

(b) *Temperature dependence.* The temperature dependence of the threshold intensity of the 468-cm^{-1} mode is shown in Fig. 5(b) for right-circularly-polarized pump light in left-handed optically active quartz. The threshold intensity is normalized to the threshold intensity $[I_r^{\text{th}}(0)]_{132\text{ cm}^{-1}}$ of the 132-cm^{-1} mode for $T \rightarrow 0$ K. The open rectangles are the experimental points. The dashed-dotted line represents the normalized spontaneous Raman linewidth of the 468-cm^{-1} mode.^{5,11} The 468-cm^{-1} mode could be observed only in a narrow temperature range between 55 and 70 K. Below 55 K stimulated Raman scattering of the 132-cm^{-1} mode occurs and suppresses the 468-cm^{-1} mode. Above 70 K our quartz crystal was damaged because of the high pump-laser intensity.

For linearly polarized pump light SRS from the 468-cm^{-1} mode could be observed in the temperature range between 30 and 70 K because of the higher Raman threshold of the 132-cm^{-1} mode [see Fig. 5(a)]. The Raman threshold of the 468-cm^{-1} mode was nearly constant within the experimental accuracy as expected from the temperature behavior of the spontaneous Raman line.^{5,11}

We estimate the ratio g_c/g_a of the Raman gain factors of the 132-cm^{-1} and 468-cm^{-1} modes from the crossing point T_c of the Raman threshold intensities of both modes. For right-circularly-polarized pump light we obtain a crossing temperature of $T_c = 55 \pm 3$ K from Fig. 5(b). Numerical calculations for the Raman oscillator [Sec. II B 5(c)] yield

TABLE I. Ratios E_ξ/E_η of the principal axes of the ellipses of laser (L) and Stokes (S) light for SRS from the 468-cm^{-1} mode of α -quartz.

E_ξ^L/E_η^L	E_ξ^S/E_η^S
0	0
0.07 ± 0.05	0.07 ± 0.05
0.37 ± 0.05	0.42 ± 0.05
0.57 ± 0.03	0.60 ± 0.03
0.98 ± 0.03	0.97 ± 0.03

a crossing of the curves at 55 K for $g_c/g_a = 0.89$. Taking into account the temperature dependence of the spontaneous Raman linewidth⁵ we get $g_c/g_a \approx 3.2$ for $T \leq 10$ K.

We estimate the value of the Raman gain factor g_a of the 468-cm^{-1} mode from spontaneous Raman data. Measurements of the absolute Raman scattering cross section of this mode have been carried out at room temperature in Refs. 29 and 30. Taking into account the temperature dependence of the spontaneous Raman linewidth^{5,11} $\delta\bar{\nu}_a$, we find a value of the Raman gain factor $g_a = (1.1 \pm 0.4) \times 10^{-3}$ cm/MW for $T \lesssim 70$ K at a pump wavelength of $\lambda_L = 1.064\text{ }\mu\text{m}$.

From our measured ratio g_c/g_a we determine a Raman gain factor of the 132-cm^{-1} mode of $g_c = (3 \pm 2) \times 10^{-3}$ cm/MW for $T \leq 10$ K. It should be emphasized, however, that this value represents a lower limit since mode-pulling effects and transient effects have not been taken into account in the estimate.

2. Polarization of the Raman Stokes light

The polarization of the laser light and the stimulated Raman Stokes light was measured with quarter-wave plate QWP2 and analyzer AN as described in Sec. III A (see Fig. 2). The measured ratios E_ξ/E_η of the principal axes of the ellipses of the laser and Stokes light are given in Table I. $E_\xi/E_\eta = 0$ and 1 correspond to linearly and circularly polarized light, respectively. The ratios E_ξ^L/E_η^L and E_ξ^S/E_η^S are equal within the experimental accuracy in agreement with theory [Eq. (61)]. The sense of rotation of the electric field vectors of the laser and Stokes light were found to be the same.

IV. CONCLUSIONS

Stimulated Raman scattering of the 132-cm^{-1} and 468-cm^{-1} modes⁷ along the c axis (z direction) of α -quartz was investigated with a single-mode Nd:YAG laser as a pump-light source. The 132-cm^{-1} E mode and the 468-cm^{-1} A_1 mode exhibit a different behavior according to their different symmetry.

(i) 132-cm^{-1} mode. Strong variations of the threshold intensity of stimulated Raman scattering with pump-laser

polarization were found. It is lowest for circularly-polarized pump light.¹³ The observed difference in the threshold intensities of right- and left-circularly-polarized incident light is due to Raman optical activity. In the investigated temperature range between 10 and 55 K the threshold intensity increased rapidly with rising temperature due to the increase of the spontaneous Raman linewidth.⁵ For elliptically polarized laser light the polarization of the stimulated Raman Stokes light was circular, except for the case where the laser light is nearly linearly polarized. The electric field vectors of the laser and Stokes light had the opposite sense of rotation.

(ii) 468-cm⁻¹ mode. The threshold intensity of stimulated Raman scattering is nearly independent on pump-laser polarization and temperature for $T < 70$ K. No indication of Raman optical activity was found within our experimental accuracy of about 5%. The polarization of the stimulated Raman Stokes light was the same as that of the laser-pump pulse.

The experimental results were compared with calculations of stimulated Raman scattering and Raman optical activity and found to be in satisfactory agreement. For most situations the traveling-wave theory and the oscillator theory of stimulated Raman scattering yielded the same results. When a difference between both theories was found, e.g., for the absolute values and the temperature dependence of the threshold intensity of the 132-cm⁻¹ mode, the experimental results were observed to lie in between the limiting cases of the traveling-wave system and the perfect oscillator system. The experimental results correspond to an oscillator system with a reduced number of passages through the crystal because of not perfectly parallel crystal surfaces.

ACKNOWLEDGMENTS

We thank Professor A. Penzkofer for stimulating discussions and valuable suggestions. Support by the Deutsche Forschungsgemeinschaft is gratefully acknowledged.

APPENDIX: POLARIZABILITY TENSORS

The magnetic dipole polarizability tensor \vec{G}' is generally a nonsymmetric second-rank Cartesian tensor, whereas the electric quadrupole polarizability tensor \vec{A} is a third-rank tensor being symmetric in the last two indices, $A_{ijk} = A_{ikj}$. These tensors must be decomposed with respect to the irreducible representations of the point group D_3 of crystalline quartz in order to determine the nonvanishing tensor components which contribute to Raman scattering. Usually only the irreducible parts of *fully* symmetric tensors are tabulated.^{31,32} Therefore we have performed the required decomposition by standard group-theoretical procedures. The tensors considered here were written in form of direct products, $G'_{ij} = u_i v_j$ and $A_{ijk} = u_i v_j v_k$, where u_i and v_i symbolize vectors being different from one another. Linear combinations of these products transforming according to irreducible representations of D_3 were determined in the basis $x + iy, x - iy$ for the E representation and z for A_2 by applying the coupling coefficients given in the tables of Koster *et al.*³³ The resulting expressions were transformed into the basis $x, y (E)$ and $z (A_2)$, which is usually used to describe Raman scattering. Each irreducible representation occurring in the decomposition was identified by an invariant denoted by the symbols G'_a to G'_f for G'_{ij} and A_a to A_1 for A_{ijk} . Then the irreducible Cartesian tensors were expressed in terms of these invariants as given in the following.

Magnetic dipole polarizability G'_{ij} :

$$A_1: \vec{G}' = \begin{bmatrix} G'_a & 0 & 0 \\ 0 & G'_a & 0 \\ 0 & 0 & G'_b \end{bmatrix}, \quad A_2: \vec{G}'(z) = \begin{bmatrix} 0 & G'_e & 0 \\ -G'_e & 0 & 0 \\ 0 & 0 & 0 \end{bmatrix}.$$

$$E: \vec{G}'(x) = \begin{bmatrix} G'_c & 0 & 0 \\ 0 & -G'_c & G'_d \\ 0 & G'_f & 0 \end{bmatrix}, \quad \vec{G}'(y) = \begin{bmatrix} 0 & -G'_c & -G'_d \\ -G'_c & 0 & 0 \\ -G'_f & 0 & 0 \end{bmatrix}.$$

In the case of \vec{G}' being symmetric, i.e., $G'_{ij} = G'_{ji}$, G'_e vanishes and $G'_f = G'_d$.

Electric quadrupole polarizability A_{ijk} :

$$A_1: A_{xij} = \begin{bmatrix} A_a & 0 & 0 \\ 0 & -A_a & A_b \\ 0 & A_b & 0 \end{bmatrix}, \quad A_{yij} = \begin{bmatrix} 0 & -A_a & -A_b \\ -A_a & 0 & 0 \\ -A_b & 0 & 0 \end{bmatrix}, \quad A_{zij} = \begin{bmatrix} 0 & 0 & 0 \\ 0 & 0 & 0 \\ 0 & 0 & 0 \end{bmatrix},$$

$$A_2: A_{xij}(z) = \begin{bmatrix} 0 & A_i & A_j \\ A_i & 0 & 0 \\ A_j & 0 & 0 \end{bmatrix}, \quad A_{yij}(z) = \begin{bmatrix} A_i & 0 & 0 \\ 0 & -A_i & A_j \\ 0 & A_j & 0 \end{bmatrix}, \quad A_{zij}(z) = \begin{bmatrix} A_k & 0 & 0 \\ 0 & A_k & 0 \\ 0 & 0 & A_1 \end{bmatrix},$$

$$E: A_{xij}(x) = \begin{bmatrix} A_c + A_e & 0 & 0 \\ 0 & A_c - A_e & A_d \\ 0 & A_d & A_f \end{bmatrix}, \quad A_{xij}(y) = \begin{bmatrix} 0 & A_e & A_d \\ A_e & 0 & 0 \\ A_d & 0 & 0 \end{bmatrix},$$

$$A_{yij}(x) = \begin{bmatrix} 0 & A_e & A_d \\ A_e & 0 & 0 \\ A_d & 0 & 0 \end{bmatrix}, \quad A_{yij}(y) = \begin{bmatrix} A_c - A_e & 0 & 0 \\ 0 & A_c + A_e & -A_d \\ 0 & -A_d & A_f \end{bmatrix},$$

$$A_{zij}(x) = \begin{bmatrix} 0 & A_g & A_h \\ A_g & 0 & 0 \\ A_h & 0 & 0 \end{bmatrix}, \quad A_{zij}(y) = \begin{bmatrix} A_g & 0 & 0 \\ 0 & -A_g & A_h \\ 0 & A_h & 0 \end{bmatrix}.$$

In the case of A_{ijk} being fully symmetric, we have $A_b = 0$, $A_k = A_j$, $A_d = A_g$, $2A_e = A_c$, and $A_f = A_h$.

- ¹P. E. Tannenwald and J. B. Thaxter, *Science* **154**, 1319 (1966).
²P. E. Tannenwald, *J. Appl. Phys.* **38**, 4788 (1967).
³P. E. Tannenwald and D. L. Weinberg, *IEEE J. Quant. Electron.* **QE-3**, 334 (1967); J. F. Scott, *ibid.* **QE-3**, 693 (1967).
⁴I. M. Aref'ev, S. V. Krivokhizha, Yu. I. Kyzylasov, V. S. Starunov, and I. L. Fabelinskii, *Zh. Eksp. Teor. Fiz. Pis'ma Red.* **8**, 142 (1968) [*JETP Lett.* **8**, 84 (1968)].
⁵A. S. Pine and P. E. Tannenwald, *Phys. Rev.* **178**, 1424 (1969).
⁶A. S. Pine and G. Dresselhaus, *Phys. Rev.* **188**, 1489 (1969).
⁷The frequencies of the optical lattice vibrations given in this paper refer to liquid-helium temperature. The frequencies at room temperature are 128 and 466 cm^{-1} .
⁸G. Chartier and S. Biraud, *Phys. Rev. Lett.* **21**, 1641 (1968).
⁹S. Biraud-Laval and G. Chartier, *Phys. Lett.* **30A**, 177 (1969).
¹⁰S. Biraud-Laval, R. Reinisch, N. Paraire, and R. Laval, *Phys. Rev. B* **13**, 1797 (1976).
¹¹G. M. Gale and A. Laubereau, *Opt. Commun.* **44**, 273 (1983).
¹²M. Klein and M. Maier, *Opt. Commun.* **44**, 411 (1983).
¹³We adopt the convention of right handed as clockwise rotation of the electric field vector, when viewed by an observer looking in the propagation direction of light.
¹⁴L. D. Barron and A. D. Buckingham, *Ann. Rev. Phys. Chem.* **26**, 381 (1975).
¹⁵L. D. Barron, in *Optical Activity and Chiral Discrimination*, Vol. 48 of *Nato Advanced Study Institutes Series*, edited by S. F. Mason (Reidel, Dordrecht, 1979), p. 219.
¹⁶L. D. Barron and A. D. Buckingham, *Mol. Phys.* **20**, 1111 (1971).
¹⁷P. W. Atkins and L. D. Barron, *Mol. Phys.* **16**, 453 (1969).
¹⁸S. F. Mason, *Adv. Infrared Raman Spectrosc.* **8**, 283 (1981).
¹⁹J.-L. Oudar, C. Minot, and B. A. Garetz, *J. Chem. Phys.* **76**, 2227 (1982).
²⁰M. Maier, *Appl. Phys.* **11**, 209 (1976).
²¹M. Born, *Optik*, 3rd ed. (Springer, Berlin, 1972), p. 403.
²²B. V. Bokut', A. N. Serdyukov, and F. I. Fedorov, *Kristallografiya* **15**, 1002 (1970) [*Sov. Phys.—Crystallogr.* **15**, 871 (1971)].
²³M. H. Grimsditch, A. K. Ramdas, S. Rodriguez, and V. J. Tekippe, *Phys. Rev. B* **15**, 5869 (1977).
²⁴J. D. Masso, C. Y. She, and D. F. Edwards, *Phys. Rev. B* **1**, 4179 (1970).
²⁵I. I. Kondilenko, P. A. Korotkov, and V. A. Klimenko, *Opt. Spektrosk.* **40**, 704 (1976) [*Opt. Spectrosc. (USSR)* **40**, 402 (1976)].
²⁶G. R. Fowles, *Introduction to Modern Optics*, 2nd ed. (Holt, Rinehart and Winston, New York, 1975), p. 53.
²⁷L. I. Katzin, *J. Phys. Chem.* **68**, 2367 (1964).
²⁸See, e.g., M. V. Klein, *Optics* (Wiley, New York, 1970), p. 488.
²⁹P. E. Schoen and H. Z. Cummins, in *Proceedings of the Second International Conference on Light Scattering in Solids*, edited by M. Balkanski (Flammarion, Paris, 1971), p. 460.
³⁰W. D. Johnston, Jr., I. P. Kaminow, and J. G. Bergman, Jr., *Appl. Phys. Lett.* **13**, 190 (1968).
³¹J. A. Salthouse and M. J. Ware, *Point Group Character Tables* (Cambridge University Press, Cambridge, 1972).
³²R. Loudon, *Adv. Phys.* **13**, 423 (1964).
³³G. F. Koster, J. O. Dimmock, R. G. Wheeler, and H. Statz, *Properties of the Thirty-Two Point Groups* (Massachusetts Institute of Technology Press, Cambridge, Mass., 1963).